View metadata, citation and similar papers at core.ac.uk

brought to you by CORE

provided by City Research Online

Rockenbach, A., Mikulich, V., Bruecker, C. & Schnakenberg, U. (2015). Fluid transport via pneumatically actuated waves on a ciliated wall. Journal of Micromechanics and Microengineering, 25(12), 125009.. doi: 10.1088/0960-1317/25/12/125009

CITY UNIVERSITY LONDON

City Research Online

Original citation: Rockenbach, A., Mikulich, V., Bruecker, C. & Schnakenberg, U. (2015). Fluid transport via pneumatically actuated waves on a ciliated wall. Journal of Micromechanics and Microengineering, 25(12), 125009.. doi: 10.1088/0960-1317/25/12/125009

Permanent City Research Online URL: http://openaccess.city.ac.uk/15771/

Copyright & reuse

City University London has developed City Research Online so that its users may access the research outputs of City University London's staff. Copyright © and Moral Rights for this paper are retained by the individual author(s) and/ or other copyright holders. All material in City Research Online is checked for eligibility for copyright before being made available in the live archive. URLs from City Research Online may be freely distributed and linked to from other web pages.

Versions of research

The version in City Research Online may differ from the final published version. Users are advised to check the Permanent City Research Online URL above for the status of the paper.

Enquiries

If you have any enquiries about any aspect of City Research Online, or if you wish to make contact with the author(s) of this paper, please email the team at publications@city.ac.uk.

FLUID TRANSPORT VIA PNEUMATICALLY ACTUATED WAVES ON A CILIATED WALL

A Rockenbach[1], V Mikulich[2], Ch Brücker[2*], and U Schnakenberg[1]

[1]Institute of Materials in Electrical Engineering 1, RWTH Aachen University,
Sommerfeldstraße 24, D-52074 Aachen, Germany
rockenbach@iwe1.rwth-aachen.de, phone: +49 241 80 27766
schnakenberg@iwe1.rwth-aadchen.de, phone: +49 241 80 27842

[2]Institute of Mechanics and Fluid Dynamics, TU Bergakademie Freiberg,
Lampadiusstrasse 4, D-09595 Freiberg, Germany
Vladimir.Mikulich@imfd.tu-freiberg.de, phone: +49 3731 39 4133
bruecker@imfd.tu-freiberg.de, phone: +49 3731 39 3833
*current address: City Univ. of London, email: christoph.bruecker@city.ac.uk

Abstract

To manipulate fluids actively a pneumatically actuated micro membrane device is developed to generate a directed transversal fluid transport in a liquid layer next to the wall. The biomimetic approach is based on the principle of cilia-type arrays that generate a mean flow by travelling wave activation. Rows of long flaps, which mimic the comb row of a ctenophore, are positioned off-centre along a row of cavities. Each cavity is covered by a flexible membrane that supports the flaps. The membranes with the flaps on top are deflected by applying a well-defined pressure profile to the cavities under the membranes such that an individual beat can be generated for each flap. Flow visualization experiments were carried out under the conditions of travelling waves. The results show a mean velocity profile that resembles that of a wall-jet. Mixing effects with increased retention times of the fluid occur in the vicinity of the membrane surfaces.

1. Introduction

One of the challenges in microfluidic devices is to propel fluids or particles through channels. A couple of known transportation methods in closed channels through physical forces, e.g. pressure driven flow [1], electrophoresis [2], dielectrophoresis [3], or surface acoustic wave devices, exist [4]. In some cases, however, particle transportation in open channels is required. Here, the methods mentioned above may fail, because of the absence of a cover plate.

For applications, like automated cleaning of artificial respiratory systems, damage-free blood cell transport near surfaces or active antifouling, mechanisms of transportation can be adopted from nature. Ciliated surfaces, e.g. in the respiratory tract [5] or in the Fallopian tube are known [6]. Cilia are also used as propelling mechanism for microorganisms, e.g. Mesodinium rubrum, Paramecium, Volvox, Chlamydomonas reinhardtii, Ctenophore or Pleurobrachia pileus [7, 8]. These cilia arrays often move in a synchronized manner with a certain phase shift between the neighbour cilia to optimize transportation of the medium close to the cilia or to generate self-propulsion of the microorganisms. The concrete actuation principle of the cilia can vary with the different species.

In the biomimetic approach to mimic biological cilia, different actuation principles of artificial cilia were developed in the last decade, using electrostatic forces, magnetic field, light-excitation, or mechanical forces for example. As a short overview, significant publications are briefly reviewed: electrostatically actuated cilia were fabricated using a bimorph approach of a thin chromium layer under a thin polyimide layer [9, 10]. The activation of electric current through underlying electrodes allows electrostatic actuation. The disadvantage of this approach is the application of high electric fields to the fluid causing electrohydrodynamic and electrolysis effects. Thus, only non-conducting fluid can be used. Likewise, artificial cilia using the magnetic-actuated concept were fabricated by dissolution of superparamagnetic nanoparticles in polydimethylsiloxane (PDMS)-based cilia structures [11–15]. However, large and expansive rotating permanent magnet arrangements are necessary to enable a deflection of this cilia type. Furthermore, artificial cilia made of an assembly of superparamagnetic colloidal particles were developed, which are held together only by magnetic forces. [16] To actuate these cilia six electromagnets have been positioned around the chip, which increased the complexity of the system.

Optically addressed artificial cilia based on self-organizing liquid-crystal polymer network actuators were published by Van Oosten et al. [17]. By using different inks, mm-sized actuators with different subunits were ink-jet printed, which can be selectively addressed by changing the wavelength of the light. Hydrogel-based cilia were fabricated by using a soft-lithography approach, yielding a reversible cilia-bending by pH-value change [18]. Recently, Sareh et al. presented an artificial cilium based on electro active polymers which are connected to a finite number of flexible elements [19]. Sanchez et al. published an approach composed of oscillatory active multimeric streptavidin, taxol-stabilized microtubules, and molecular biotin-labelled kinesin motors, which self-assemble into active bundles, thus exhibiting patterns reminiscent of those found in eukaryotic cilia and flagella [20]. Dayal et al. presented artificial cilia formed by chemo-responsive gels. These gels can undergo the

Belousov-Zhabotinsky reaction, thus form autonomous self-oscillation of periodic swelling and crescendo [21].

However, the fabrication processes of all shown approaches suffer from high costs, complexity and non-mainstream technologies, preventing a cost-effective production. On the contrary, soft-lithography and micro-moulding of polydimethylsiloxane (PDMS) are established techniques for the production of low-cost microfluidic devices. Ideally they can be used for the fabrication of flexible membranes and flaps. Several papers presented pneumatically driven refreshable Braille-type cell arrays as tactile display prototypes for the blind and visually impaired by using pneumatically actuated PDMS membranes [22–24]. Mechanical activation of PDMS-based cilia arrays on flexible membranes using base-layer deformation with ball chains or piston stamps were presented by Keissner and Brücker [25, 26]. The latter were proven to generate well-defined streaming patterns, however, the mechanical principle used therein does not allow an individual addressing of the beating cycle of each cilium; thus the pattern of the wave-type excitation could only be varied in frequency but not in spatial coordinates.

The objective of this paper is to design an artificial comb row on flexible membranes using pneumatically based actuation and the characterization of fluid transport close to the comb row in uncapped channels. The basic concept was already published in [27]. The actuation principle is sketched in Figure 1. Rows of cilia-like flaps are positioned on flexible membranes out of the centre of regularly separated cavities. Each flap can be deflected separately by an induced pneumatic pressure from the underside of the cavity, which then leads to a bending of the supporting membrane. Owing to the high aspect ratio of the flaps the membrane deflection results in a considerably large transversal motion of the flap tips. Furthermore, this motion is only driven by the movement of the membranes, and not by bending the flaps. In addition, as a reaction to the pressure profile, the outward motion may differ in the temporal profile from the inward motion of the membrane, thus imposing an asymmetry in the temporal motion cycle between the forward and backward directed stroke. The bending cycle between adjacent cavities can be controlled by addressing the individual pressure tubes to produce a traveling wave.

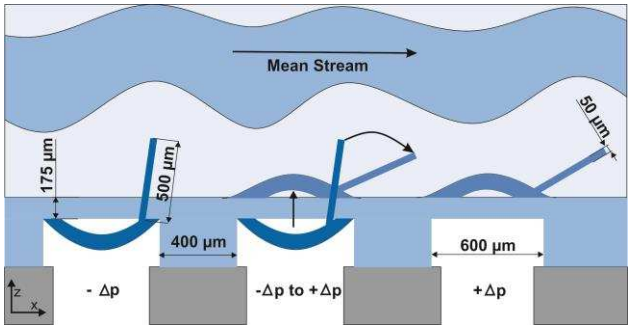

Fig. 1: Concept of the pneumatically actuated cilia array (cross-section, not to scale): rows of flaps are located off-centre on flexible membranes. *The pressures* Δp *to deflect the membranes* is individually applied to the underlying channels. Design details: the pressure channel (cavity) under the 175 µm thick membranes is 600 µm wide. In combination with the 400 µm wide supporting structure between two channels a pitch of 1000 µm is defined. The flaps are 500 µm in height, 50 µm thick and 20 000 µm long in span, respectively. In difference to the upright version presented in [27], the flaps here are tilted by 45°. The forward stroke is generated by the pressure change from low to high pressure in the cavity. The recovery stroke is done vice versa.

2. Design Concept

The first design introduced in [27] is comprised of non-continuous flaps on top of the membranes to study the behaviour of span wise mixing. However, detailed flow measurements of the flow profiles were impossible to obtain due to obstruction effects.

The present work is focused on continuous flaps and their efficiency in generating homogeneous directional transport. The new setup offers optical access from the side and top to measure the velocity profiles. An improvement was introduced by tilting the flaps by 45° in order to provoke further symmetry breakage in the beating pattern. Layout details of the membrane and the flap structure are shown in Figure 1. The width of the supporting structure was set to 400 µm and the width of the cavity to 600 µm, respectively. Typically, 500 µm high (h_{flaps}) and 50 µm wide flaps were used as artificial rows of flaps that extend into the fluid from the flexible surface. The flaps extend over a large span of 20 000 µm. These large dimensions were chosen to enable a detailed high-resolution characterization of fluid velocities between and above the rows of flaps.

For all experiments deionized water was used as fluid. The Reynolds-number of the beating flap is of order of O(10), which corresponds to the flow regime, were Ctenophora live in.

To move the fluid effectively at low Reynolds-numbers an asymmetric movement is required, which is realized by the following features:

First of all, the time responses of the two stroke phases differ from another. This is due to the difference in pressure in the cavity affected by the magnitude and direction of the pressure pulse, the fluid impedance and the resistance of the pressure tubes. The base level of the membrane is defined when all cavities are connected to the low pressure. A forward stroke is generated when one valve switches the pressure level from low to high pressure for a short period of time. When the valve is retracted to its original position (low pressure level) the motion is reversed and the flap tilts backwards to its base level position. Figure 2 shows the pressure profiles measured within one single cavity. The discontinuous blue curve refers to the valve position and reflects the switching behaviour of the valve. The measured pressure change in the cavity from low to high level is significantly fast. Here, a pressure change from -0.6 bar to +0.6 bar lasts 36 ms, which is referred to the power stroke. After switching back from high to low pressure level at the valve, the pressure in the cavity decreases until it reaches the lower level. This drop follows an exponential decay and takes a considerably longer time-span in contrast to the high jump phase. A decrease from +0.6 bar to -0.6 bar in the cavity lasts 66 ms. This means that the forward stroke is roughly two times faster than the backward stroke. Therefore we differ the forward directed “power“ stroke from the backward directed “recovery” stroke, thereby following the notation used in biology. The timing order of the succession of beating cycles along the surface is then a further parameter to generate travelling waves, see Fig 3, in which each individual flap is showing the same motion pattern as given in Figure 4. A typical tip speed is then the tip excursion (350µm) divided by the power stroke period (36ms) which is roughly $u_{Tip}\approx 10$mm/s. The Reynolds-number defined with the tip velocity and the height of the flap is then $Re\approx 5$ while for the recovery stroke it is only half of that. In consequence, the drag

force for the power stroke is larger than that of the recovery stroke, therefore a net flow is expected in the direction of the power stroke.

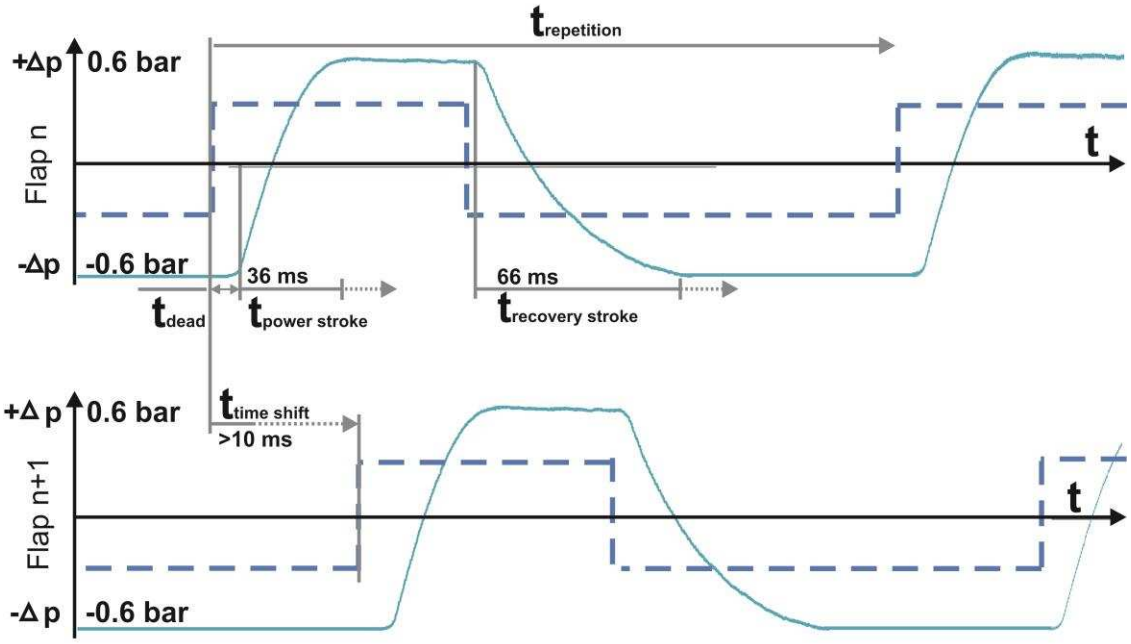

Fig. 2: Pressure profiles beneath two neighbouring membranes. The discontinuous blue line shows the valve-position, and the light blue line corresponds to the measured pressure under the membrane. t_{dead} marks the dead time between the opened valve and the starting pressure rise, which is about 8 ms. $t_{power\ stroke}$ is the time used to switch from low to high pressure, which lasts 36 ms. $t_{recovery\ stroke}$ is the time used to switch from high pressure back to low pressure, which lasts 66 ms. The repetition time $t_{repetition}$ varies between 200 ms and 1000 ms. Between two adjacent flaps a time shift $t_{time\ shift}$ of 20 or 50 ms is applied, respectively.

The custom-made pneumatic triggering module in combination with the valves (see chapter 3) is capable of switching all valves completely independent from each other. To create a travelling wave mechanism in the flap array, pressure was switched from +0.6 bar to -0.6 bar to all of the twenty membranes consecutively. One wave can be made up of 20 flaps, 10 flaps or 5 flaps ($n_{flaps\ per\ wave}$). The wavelength results in:

$$l_{wave\ length} = n_{flaps\ per\ wave} * l_{pitch}, \qquad 1$$

with l_{pitch} being the distance between to flaps, which is 1000 µm.

In the present setup, the "on" time of the valve $t_{valve\ on}$ can be set to a minimum of 36 ms without reduction of the applied pressure level, which corresponds to a maximum frequency of 9.8 Hz. This limit is defined by the length of recovery and power stroke. In general, a much lower frequency is defined to keep the movement well defined. The valves were switched on for 40 and 100 ms. A duty cycle D of 10 and 40% is defined, with respect to the "off" time $t_{valve\ off}$:

$$D = \frac{t_{valve\ on}}{t_{valve\ on} + t_{valve\ off}} \qquad 2$$

The propagation velocity of the wave depends on the pitch l_{pitch} between two flaps and the applied time shift t_{shift}. The wave velocity v_{wave} can be defined as:

$$v_{wave} = \frac{l_{pitch}}{t_{time\ shift}} \qquad 3$$

The beating of a flap is defined by two parameters, the "on" time $t_{valve\ on}$ and "off" time $t_{valve\ off}$ of the valve. From these parameters the beating frequency $f_{beating}$

$$f_{beating} = \left(t_{valve\ on} + t_{valve\ off}\right)^{-1} = \left(t_{repetition}\right)^{-1} \qquad 4$$

is derived.

Figure 3 shows a snapshot picture of a wave travelling through the fluid channel (side view) with the applied pressures to each membrane. A section of 8 flaps is shown and one wave is visible in the middle. In the experiments 1, 2 or 4 waves were applied to the whole device consisting of 20 membranes.

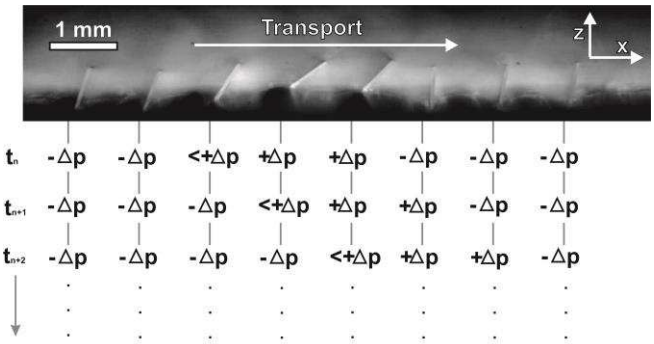

Fig. 3: Travelling wave chronology. The traveling wave is applied from left to right, as the flaps are numbered. Effective stroke (high pressure) is applied on flap 4 and 5. At flap 1 the membrane deformation as well as the flap deflection corresponds to the application of the recovery stroke. The vertical lines mark the pressure level at the individual position of each membrane-flap combination. Pressure changes with time. Between t_n and t_{n+1} a time increment of $t_{phase\ shift}$ was adjusted.

In addition, the path of the flap tip is asymmetric. When a pressure change is applied to one single cavity from low to high pressure, the resulting motion pattern of the flap resembles a power stroke of the flap. Owing the interaction of the cavity pressure with the support structures and the material parameters of the elastomer, the change in pressure back to low levels leads to a slightly different path of the flap tip during membrane relaxation and inversion. This is depicted in Figure 4 by means of the measured path of the tip in the forward (red line) and backward (dashed black line) motion phase. There is a clear indication of hysteresis: in the forward stroke the flap tip reaches deeper into the fluid, while in the retrace phase of the flap the tip follows a path closer to the wall. The total height difference on the 342 µm long path was determined to be 85 µm, which corresponds to 17 % of the flap height.

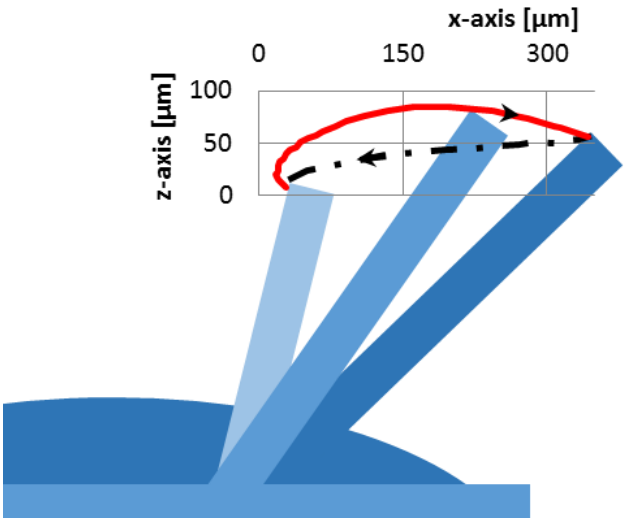

Fig. 4: Schematic view of the flap movement with the measured path of a flaps tip. The upper path represents the fast power stroke whereas the lower path corresponds to the slow recovery stroke. In the upper path high-pressure whereas in the lower path low-pressure is applied. The data were obtained from measuring the flap deflection optically

under a pressure application of -0.6 bar to +0.6 bar.

Compared to natural cilia the achieved relative deflection normalized to the cilia height is smaller in this artificial approach. In nature, the length of a typical complete stroke is 1.6 to nearly double the height of the cilium itself [28], whereas with our artificial cilia a movement of 450 µm was realized, corresponding to a ratio of 0.9. This is comparable to other artificial systems like those published by Den Toonder et al. [9, 10] with a ratio of 0.4, and those reported by Shields et al., Fahrni et al. and Brennen et al. [12, 13, 29] with a ratio of 0.9 to 1.24, as well as Pokroy et al. and Brennen et al. [18, 30] with a ratio of about 1. Only Timonen et al. achieved a higher ratio of about 2, but without further report about the details of the induced flow [15].

Note, that a quantitative comparison of flow transport effectiveness between the different artificial cilia approaches is difficult since they use different scales, beating patterns and wave characteristics. The herein presented concept is not designed to investigate the flow in the very limit of the Stokes-regime but to cover also the condition where Ctenophore and Pleurobrachia pileus are generating transport. This is at Reynolds-number of order of O(10) where inertia effects already play a grave role. Part of the contributing factors for flow transport is therefore the difference in speed of the power- and recovery stroke as explained above. Another but probably only small contribution might come from the hysteresis in the motion of the flaps. In the power stroke the flaps extends farther in the flow than in the recovery stroke. Therefore, the effective area generating the momentum transfer is larger in the power stroke than in the recovery phase.

3. Materials and methods

The foil was fabricated from PDMS (Sylgard 184, Dow Corning, Midland, USA) using standard UV lithography and soft-lithography techniques in combination with SU-8 micro moulds. Two moulds are needed. For the first one the process flow is schematically shown in Figure 5. First, a 100 mm borosilicate glass wafer was coated and structured with an evaporated chromium layer serving as a mask [31] (Figure 5A). Five 100 µm SU-8-layers (MicroChem, Newton, USA) were consecutively spun onto the chromium-side of the wafer (front side) using a RC-8 spin coater with a Gyrset top frame (Süss MicroTec, Garching, Germany). Soft-bakes were carried out after each deposition step. The resulting 500 µm thick SU-8 layer was exposed to a light density of 500 mJ/cm² from the backside of the wafer using a Süss MicroTec MA6 mask aligner (Figure 5B). This ensures a high slew rate of the SU-8 structures which is necessary to peel-off the casted PDMS from the SU-8 moulds later on. After a post-exposure bake (six hours at 50°C and six hours at 65°C) a sixth 100 µm thick SU-8 layer was spun on the front side of the wafer and exposed using a mask followed by the post-exposure bake described above. All six SU-8 layers were wet-chemically developed in a mr-dev 600 (MicroChem) in one step (Figure 5C). The first five sublayers form the mould for the flaps. The top sixth SU-8 layer forms spacers to define the membrane thickness. Finally, the developed wafers were coated with a 1 µm thick Parylene-C layer (PDS 2010, SCS Specialty Coating Systems, Indianapolis, USA) serving as a non-sticking coating.

The second mould is needed to form the channels beneath the membranes. The fabrication process is similar to the fabrication process of the first mould. The

top layer defines self-alignment structures fit to the first mould and align the two moulds to each other (Figure 5D). Using this alignment method the undesirable rotation from one mould to the other was reduced to +/- 0.05°.

Subsequently, PDMS was prepared according to the manufacturer's instructions by vacuum mixing and casted on top of both wafers (Figure 5E). The casts were evacuated for 15 minutes at 100 mbar to remove bubbles in small cavities. The two moulds were moved slowly towards each other starting at one side and pushing the surplus silicone out on the other side (Figure 5F). The assembled parts were cured at 60°C for one hour (Figure 5G).

The cured silicone was first peeled-off from the membrane forming mould (Figure 5H) and then from the cilia forming mould (Figure 5I). To carry out a reproducible peeling process the membrane has to have a minimum thickness of 100 µm.

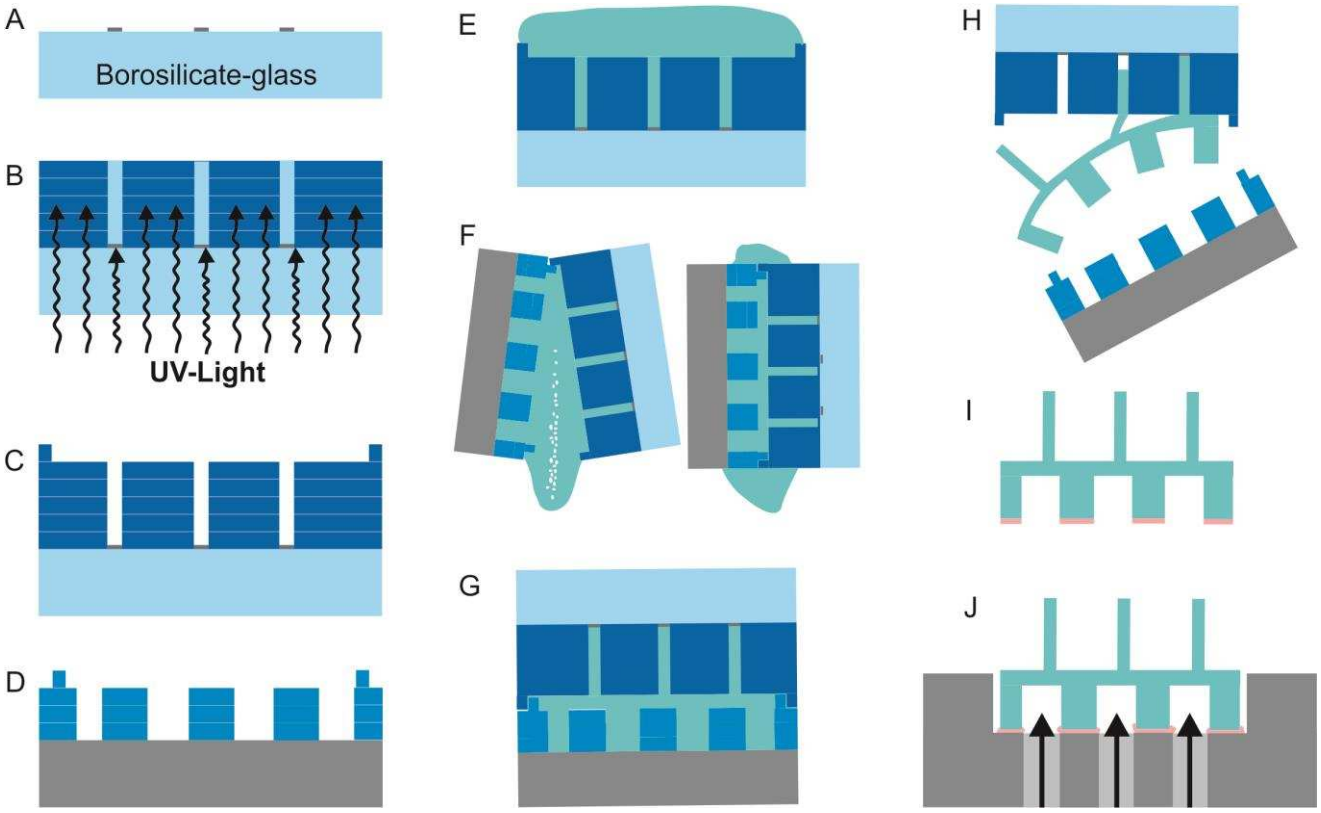

Fig. 5 Process flow for the fabrication of the biomimetic particle transporter chip. Two moulds are needed. A) Glass wafer with chromium layer (front side). B) Consecutive deposition of several SU-8 layers, soft-bake and UV exposure from the back side. C) Deposition of an additional SU-8 layer defining the membrane thickness in the first mould and serving as an adjustment structure for the assembly in the second mould (D). E) Casting of PDMS on both moulds. F) Pushing the two moulds together. G) Curing. H) Peeling off the cured silicone from the two moulds. I) Silicone part with a thin film of silicone glue. J) Silicone part assembled to the connector. For detailed description the reader is referred to the text.

The silicone foil is glued to an aluminium connector of the macroscopic valve system containing feed-throughs, so that each membrane can be addressed individually with pressure, using a standard micro con-

tact printing technology with MED1-4013 glue (Nusil Technology, Sophia Antipolis, France) diluted 1:2 in cyclohexane spun on the wafer (Figure 5J). After bonding, the compound was finally cured twelve hours in an oven at 60°C.

Figure 6 shows the complete silicone device. Transparent 30 mm long membranes are arranged in 20 rows laterally with a pitch of 1 mm. On top of each membrane a 20 mm long flap is arranged.

To tilt the flaps and reach an angle of 45° the flaps were pushed to one side and pressed down completely using a glass slide and a weight of 400 g. The PDMS used must be bended directly after curing. To do that a glass slide is positioned at one side of the foil and pushed to the other side, so that all flaps are tilted one by one. Then the slide was fixed and bended at 80°C for 1.5 hours in an oven. The last step is to lift up the flaps from the foil, to prohibit further bending.

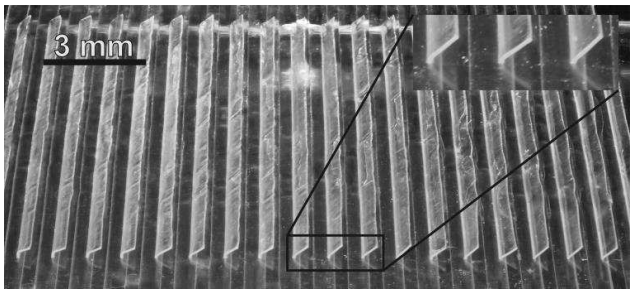

Fig. 6: Photograph of the artificial comb row array. 20 rows of flaps are located on flexible membranes (not shown while on the back side). Each channel is 30 000 µm long. On each membrane a 20 000 µm long and tilted flap is located.

The pressure under the membranes was applied with the aid of a custom-made valve system using MHP1-M4H 3/2-way-valves (Festo, Esslingen, Germany) having a switching time of about 4 ms. The valve system was controlled by a NI cRio-9074 control unit (National Instruments, Austin, USA). The valves switch the pressure from +0.6 bar to -0.6 bar. The high pressure and low pressure is applied from pressure reservoirs. Phase shifts between two adjacent membranes establish a travelling wave mechanism. If the traveling wave is moving in the direction of the power stroke the wave is called “symplectic”, while it is named “antiplectic” when applied in the reverse direction. The transport behaviour was studied using the method of particle tracing. Polystyrene particles with an average size of about 50.7 µm +/- 0.7 µm (Microparticles, Berlin, Germany) were used.

4. Results and Discussion

Particle pathlines were visualized by superposition of a series of pictures taken at the same phase within the traveling wave cycle. Figure 7 shows a superposition of 205 pictures with a time shift of 200 ms. Differences in particle velocity can be calculated by measuring the distances between two pictures of the same particle. In the superposed image slow particles were characterized by continuous lines and fast particles by discontinuous lines. The overall particle transport was always from left to right in the direction of the power stroke, for comparison see Figure 1. The lens focus was set to the centre of the channel such that a larger number of particles above the flaps were in focus. The upper interface from the liquid layer to the surrounding air was set to a height of 12 times the height of a flap within the channel. A typical measured flow profile is shown in Figure 7 (parameter-set: symplectic wave, frequency 5 Hz, duty cycle 25%, wave velocity 100 mm/s and wave length 20 mm). The red line characterizes the horizontal velocity component and the white curve represents a fit curve

of the flow profile. A maximum particle velocity of 426 µm/s was calculated, whereas the mean velocity in x-direction was 188 µm/s. The average sedimentation velocity in z-direction was determined to be 14 µm/s.

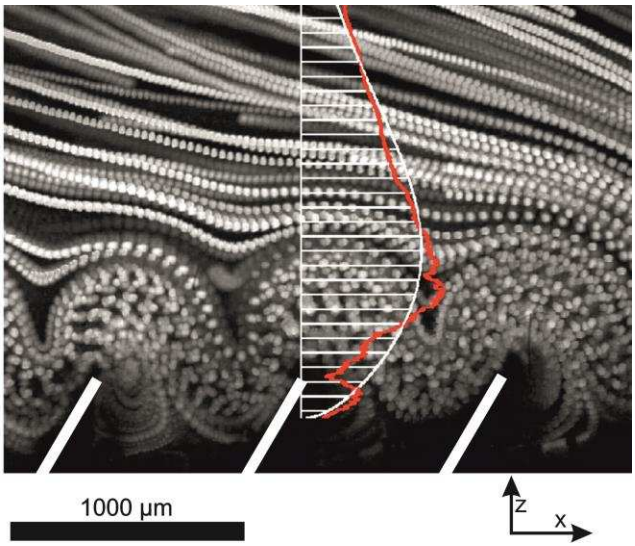

Fig. 7: Superposed phase-locked images (in side view) of a membrane and flap arrangement. The focus is set to the first third of the flap row. The images are superposed from a series of 205 individual pictures taken at the same phase within the wave cycle. Parameter-set: frequency 5 Hz, duty cycle 25%, wave velocity 100 mm/s and wave length 20 mm. The white curve represents a fit curve of the flow profile (red curve).

The flow profile was fitted using a skewed Gaussian approximating of a typical wall-jet profile [32]. The fit shows the characteristics of a wall-induced transport like a wall-jet. With the flaps tilted by 45°, the mean transport velocity by our device was increased by a factor of 8 in comparison to the vertical flap arrangement [27].

In general, at a larger distance from the wall ($> 2\ h_{flap}$) the recorded flow patterns illustrate a rather homogenous transversal transport from left to right in direction of the power stroke. In contrast, large vertical up- and downwards motion is formed because of the cilia beating cycle near the flaps. The phase-averaged path lines show a curved flow around the tips of the flaps, which is similar for all rows of flaps.

The measurements were also repeated with the travelling waves running in reverse direction (antiplectic) while retaining other boundary conditions. The observed transport was still in direction of the power stroke. This implies that fluid transport direction is mainly defined by the flap tilt. We rotated the device by180° around the vertical axis and observed reverse of flow direction, this let us conclude that there were no external disturbances affecting the flow direction. Finally, we tested the transport with synchronous flapping while all other parameters were kept constant. The results shown in Fig 8 clearly reveal that transport is much worse than with travelling wave motion. A possible explanation is that in case of synchronous flapping there is no phase difference in the flaps kinematics. As consequence, there is no relative motion between the neighbouring flaps. In contrast, for running waves the relative motion between neighbouring flaps causes a considerable squeeze flow in the gaps as seen in the particle trace visualizations between the flaps in Figure 7. This is concluded to be the reason for a much slower fluid propelling at synchronous flapping. In addition, we observe the squeeze flow angled against the wall-normal because of the tilt of the flaps which guide the fluid out of the bottom layer. Thus, direction of the squeeze flow is given by the tilt of the flaps and contributes to the transversal flow generated in the upper layer. In comparison, direction of the travelling wave - either symplectic or antiplectic – therefore seemingly does not affect the direction of overall flow transport, as seen in Figure 8. However,

the speed of the transversal fluid transport at symplectic wave propagation was in any case higher than for antiplectic propagation at otherwise unchanged conditions. This is attributed to the potential effect known as the waving plate mechanism, as described by Wu [33]. Though the flow in our case is at low Reynolds-numbers, there is still considerable influence of inertia that might explain the difference in mean transport speed at the different directions of wave vectors.

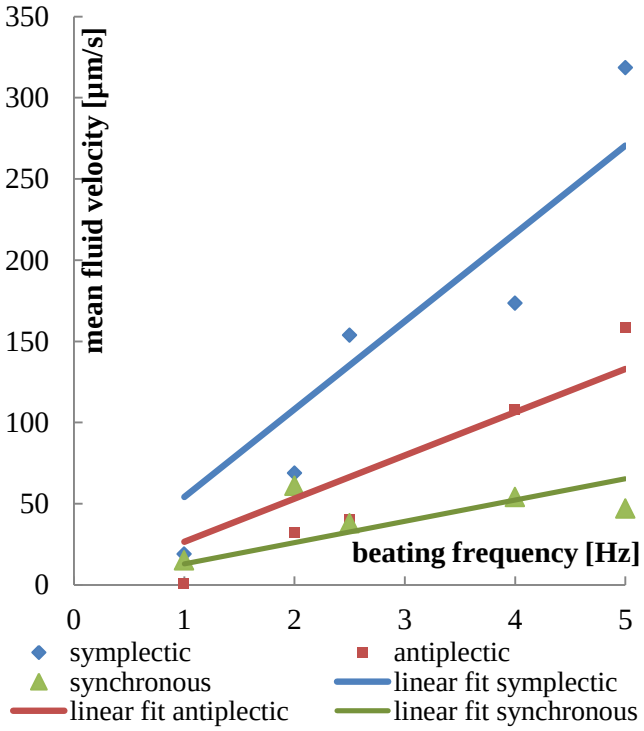

Fig. 8: Mean fluid velocity with respect to beating frequency of the flaps, while the Reynolds number was constant. Exact values are given in Table 1.

What else is seen in Figure 8 is the clear tendency of increased transversal speed with increasing beating frequency. Again, the Reynolds numbers for both strokes are kept constant. The corresponding parameter sets are listed in Table 1 in the Annex. A frequency of 5 Hz is the highest beating frequency for which reasonable results were achieved with the device.

This tendency agrees with the observations by Dauptain et al. [28] regarding a simulated beating comb row of the ctenophore Pleurobrachia pileus at frequencies between 5 and 25 Hz. They reported a peak velocity of about 70 mm/s for 2 mm long flaps at 25 Hz. Vilfan et al. (magnetic particles chains 31 µm long [16]) reported a velocity of 3.3 µm/s in their systems. The device developed by Shields (magnetic nanorods, 25 µm long) realized a transport velocity of 200 µm/s at 5 Hz, which is also propelled by magnetic fields [13]. Toonder et al. reported, a peak velocity of 600 µm/s with their microparticle chains for their 100 µm long cilia [9]. However, these magnetically driven devices were mainly used for mixing and not for homogeneous transport. Again, note that a quantitative comparison between the different artificial cilia devices is difficult because of the largely differing flap shapes, motion patterns, flow conditions and wave parameters, if any waves are involved.

5. Conclusion

A travelling wave concept was introduced for directional fluid transport near a ciliated wall by pneumatic actuation. With this approach a device was realized which is able to generate a homogeneous fluid transport with substantial flow velocities near the wall. Silicone flaps mimicking a comb row of ctenophore Pleurobrachia pileus were positioned on a flexible membrane and actuated individually through application of pneumatic pressure from the underside. The repeated application of travelling waves along the rows of cavities induced a continuous net flow above

the flap tips in direction of the power stroke, for both the symplectic and the antiplectic case. Another factor of importance is the tilt of the flaps and its effect on the directional guidance of the squeeze-flow that is generated in the gap between neighbouring flaps. It is assumed that this effect contributes to the observed net flow directed always along the power stroke. As expected, flow speed increases with beating frequency, too. For our device maximum velocities (flaps with 500 µm height) were observed at beating frequencies of 5 Hz, which resulted in a mean velocity of 319 µm/s. In comparison to other concepts using artificial cilia, this device produces a homogeneous transport and is more flexible in size and actuation. In addition, during long-term experiments over one week the device did not show any symptoms of fatigue. Detailed investigations of the flow profiles between and above the comb rows provide guidelines for downscaling the device to relevant microfluidic geometries making the concept attractive and promising for uncapped system applications, where defined flow profiles or mixing with high retention times are needed. For use in real microsystems the dimensions can easily be reduced by redesign in combination with 3-D-printing of the moulds.

6. Acknowledgements

Funding was granted by the German Federal Ministry of Education and Research under grant #16SV5341 (PaTra) and German Research Foundation DFG, grant # SCHN 587/15-1 and BR 1494/30-1 within the priority program "Microswimmers". We gratefully acknowledge the funding and the cooperation with our project partners P. Uhlmann, A. Rollberg, and M. Kunder from Leibniz Institute of Polymer Research Dresden e.V. - Dept. Physical Chemistry und Polymer Physics, Dresden, Germany. Gerhard Bleidiessel from microresist technology MRT, Berlin, Germany, is gratefully acknowledged for his outstanding support and discussions relating to SU-8 processing challenges.

7. References

[1] Squires TM, "Microfluidics : Fluid physics at the nanoliter scale," Rev. Mod. Phys., vol. 77, no. July, pp. 977–1016, 2005.

[2] Wu D et al., "Electrophoretic separations on microfluidic chips," J. Chromatogr. A, vol. 1184, no. 1–2, pp. 542–59, Mar. 2008.

[3] Markx GH and Davey CL, "The dielectric properties of biological cells at radiofrequencies: applications in biotechnology," Enzyme Microb. Technol., vol. 25, no. 3–5, pp. 161–171, Aug. 1999.

[4] Friend J and Yeo LY, "Microscale acoustofluidics: Microfluidics driven via acoustics and ultrasonics," Rev. Mod. Phys., vol. 83, no. 2, pp. 647–704, Jun. 2011.

[5] Sleigh MA et al., "State of Art The Propulsion of Mucus by Cilia," Am. Rev. Resipratory Dis., vol. 137, no. 3, pp. 726–41, 1988.

[6] Lyons RA et al., "The reproductive significance of human Fallopian tube cilia," Hum. Reprod. Update, vol. 12, no. 4, pp. 363–372, 2006.

[7] Guasto JS et al., "Fluid Mechanics of Planktonic Microorganisms," Annu. Rev. Fluid Mech., vol. 44, no. 1, pp. 373–400, Jan. 2012.

[8] Goldstein R et al., "Noise and Synchronization in Pairs of Beating Eukaryotic Flagella," Phys. Rev. Lett., vol. 103, no. 16, p. 168103, Oct. 2009.

[9] Den Toonder JMJ and Onck PR, "Microfluidic manipulation with artificial/bioinspired cilia," Trends Biotechnol., vol. 31, no. 2, pp. 85–91, Feb. 2013.

[10] Den Toonder JM et al., "Artificial cilia for active micro-fluidic mixing," Lab Chip, vol. 8, no. 4, pp. 533–541, Apr. 2008.

[11] Khaderi SN et al., "Magnetically-actuated artificial cilia for microfluidic propulsion," Lab Chip, vol. 11, no. 12, pp. 2002–10, Jun. 2011.

[12] Shields AR et al., “Biomimetic cilia arrays generate simultaneous pumping and mixing regimes,” Proc. Natl. Acad. Sci. U. S. A., vol. 107, no. 36, pp. 15670–5, Sep. 2010.

[13] Fahrni F et al., “Micro-fluidic actuation using magnetic artificial cilia,” Lab Chip, vol. 9, no. 23, pp. 3413–21, Dec. 2009.

[14] Den Toonder JMJ, “Artic Project,” 2014. [Online]. Available: www.artic-ptoject.eu.

[15] Timonen JVI et al., “A facile template-free approach to magnetodriven, multifunctional artificial cilia,” ACS Appl. Mater. Interfaces, vol. 2, no. 8, pp. 2226–30, Aug. 2010.

[16] Vilfan M et al., “Self-assembled artificial cilia,” Proc. Natl. Acad. Sci. U. S. A., vol. 107, no. 5, pp. 1844–7, Feb. 2010.

[17] Van Oosten CL et al., “Printed artificial cilia from liquid-crystal network actuators modularly driven by light,” Nat. Mater., vol. 8, no. 8, pp. 677–682, Aug. 2009.

[18] Zarzar LD et al., “Bio-inspired design of submerged hydrogel-actuated polymer microstructures operating in response to pH,” Adv. Mater., vol. 23, no. 12, pp. 1442–6, Mar. 2011.

[19] Sareh S et al., “Swimming like algae : biomimetic soft artificial cilia,” J. R. Soc. Interface, 2012.

[20] Sanchez T et al., “Cilia-like beating of active microtubule bundles,” Science, vol. 333, no. 6041, pp. 456–9, Jul. 2011.

[21] Dayal P et al., “Chemically-mediated communication in self-oscillating, biomimetic cilia,” J. Mater. Chem., vol. 22, no. 1, p. 241, 2012.

[22] Wu X et al., “A refreshable braille cell based on pneumatic microbubble actuators,” J. Microelectromechanical Syst., vol. 21, no. 4, pp. 908–916, 2012.

[23] Richard E. Fan, Adam M. Feinman, Christopher Wottawa, Chih-Hung King, Miguel L. Franco, Erik P. Dutson, Warren S. Grundfest MOC, “Characterization of a Pneumatic Balloon Actuator for Use in Refreshable Braille Displays,” in Medicine Meets Virtual Reality 17, 2009, pp. 94 – 96.

[24] Pakazad SK et al., “A platform for manufacturable stretchable micro-electrode arrays,” Procedia Eng., vol. 47, pp. 817–820, 2012.

[25] Keißner A and Brücker C, “Directional fluid transport along artificial ciliary surfaces with base-layer actuation of counter-rotating orbital beating patterns,” Soft Matter, vol. 8, no. 19, p. 5342, 2012.

[26] Brücker C and Keissner A, “Streaming and mixing induced by a bundle of ciliary vibrating micro-pillars,” Exp. Fluids, vol. 49, no. 1, pp. 57–65, Nov. 2009.

[27] Rockenbach A et al., “Pneumatically Actuated Biomimetic Particle Transporter,” in 2014 IEEE 27th International Conference on Micro Electro Mechanical Systems (MEMS 2014), 2014, pp. 927–930.

[28] Dauptain A et al., “Hydrodynamics of ciliary propulsion,” J. Fluids Struct., vol. 24, no. 8, pp. 1156–1165, Nov. 2008.

[29] Brennen C and Winet H, “Fluid Mechanics of Propulsion by Cilia and Flagella,” Annu. Rev. Fluid Mech., vol. 9, pp. 339–98, 1977.

[30] Pokroy B et al., “Fabrication of Bioinspired Actuated Nanostructures with Arbitrary Geometry and Stiffness,” Adv. Mater., vol. 21, no. 4, pp. 463–469, Jan. 2009.

[31] Sato H et al., “An all SU-8 microfluidic chip with built-in 3D fine microstructures,” J. Micromechanics Microengineering, vol. 16, pp. 2318–2322, 2006.

[32] Hoskinson AR et al., “Force measurements of single and double barrier DBD plasma actuators in quiescent air,” J. Phys. D. Appl. Phys., vol. 41, p. 245209, 2008.

[33] Wu TY "Swimming of a waving plate", J. Fluid Mech. 10:321-44, 1961.

8. Appendix

Table 1: Parameters for different beating frequencies and corresponding velocities for antiplectic, symplectic and synchronous beating. For synchronous beating only the parameters *"*beating frequency*"* and *"*duty cycle*"* are applicable.

				Antiplectic velocity [µm/s]		Symplectic velocity [µm/s]		Synchronous velocity [µm/s]	
$f_{beating}$ [Hz]	D [%]	v_{wave} [mm/s]	$l_{wave\ length}$ [mm]	max	mean	max	mean	max	mean
1	10	20	20	14	0	48	19	25	15
2	20	20	10	153	32	152	69	98	61
2.5	10	50	20	76	40	282	154	115	38
4	40	20	5	235	108	294	174	97	54
5	20	50	10	378	159	608	319	99	47